Modeling Long-Term Temporal Variation of Dew Formation in Jordan and Its Link to Climate Change

Atashi, Nahid

2020-08

Atashi , N , Rahimi , D , Al Kuisi , M , Jiries , A , Vuollekoski , H , Kulmala , M , Vesala , T & Hussein , T 2020 , ' Modeling Long-Term Temporal Variation of Dew Formation in Jordan and Its Link to Climate Change ' , Water (Basel) , vol. 12 , no. 8 , 2186 . https://doi.org/10.3390/w12082186

http://hdl.handle.net/10138/319747
https://doi.org/10.3390/w12082186

water

MDPI

Article

Modeling Long-Term Temporal Variation of Dew Formation in Jordan and Its Link to Climate Change

Nahid Atashi [1,2], Dariush Rahimi [1], Mustafa Al Kuisi [3], Anwar Jiries [4], Henri Vuollekoski [2], Markku Kulmala [2], Timo Vesala [2,5] and Tareq Hussein [2,6,*]

1 Department of Physical Geography, Faculty of Geographical Science and Planning, University of Isfahan, Isfahan 8174673441, Iran; n.atashi@geo.ui.ac.ir (N.A.); d.rahimi@geo.ui.ac.ir (D.R.)
2 Institute for Atmospheric and Earth System Research (INAR/Physics), University of Helsinki, FI-00014 Helsinki, Finland; henri.vuollekoski@gmail.com (H.V.); markku.kulmala@helsinki.fi (M.K.); timo.vesala@helsinki.fi (T.V.)
3 Department of Geology, The University of Jordan, Amman 11942, Jordan; mkuisi@ju.edu.jo
4 Faculty of Science, Mutah University, Karak 61710, Jordan; jiries57@hotmail.com
5 Faculty of Agriculture and Forestry, Institute for Atmospheric and Earth System Research (INAR/Forest), University of Helsinki, FI-00014 Helsinki, Finland
6 School of Science, Department of Physics, University of Jordan, Amman 11942, Jordan
* Correspondence: tareq.hussein@helsinki.fi

Received: 3 July 2020; Accepted: 30 July 2020; Published: 3 August 2020

Abstract: In this study, we performed model simulations to investigate the spatial, seasonal, and annual dew yield during 40 years (1979–2018) at ten locations reflecting the variation of climate and environmental conditions in Jordan. In accordance with the climate zones in Jordan, the dew formation had distinguished characteristics features with respect to the yield, seasonal variation, and spatial variation. The highest water dew yield (an overall annual mean cumulative dew yield as high as 88 mm) was obtained for the *Mountains Heights Plateau*, which has a Mediterranean climate. The least dew yield (as low as 19 mm) was obtained in *Badia*, which has an arid climate. The dew yield had a decreasing trend in the past 40 years due to climate change impacts such as increased desertification and the potential of sand and dust storms in the region. In addition, increased anthropogenic air pollution slows down the conversion of vapor to liquid phase change, which also impacts the potential of dew formation. The dew yield showed three distinguished seasonal patterns reflecting the three climates in Jordan. The *Mountains Heights Plateau* (Mediterranean climate) has the highest potential for dew harvesting (especially during the summer) than *Badia* (semi-arid climate).

Keywords: cumulative dew; spatial variation; seasonal variation

1. Introduction

Climate change impacts on water resources and supplies. Disruption of water supplies has socio-economic consequences that might take many years to recover. By the year 2025 more than 50% of the world population will suffer from freshwater supplies [1]. Therefore, awareness, international agreements, and national strategies are built up worldwide to wisely manage and restore water resources on both local and regional scales [2]. Technological advancement also plays an important role in decreasing the effects of climate change on water resources. For example, water desalination has been utilized whenever it is affordable to produce fresh water. Alternatively, cloud seeding by injecting cloud condensation nuclei (CCN) or ice nuclei (IN) in the atmosphere may also help in improving rain patterns in some semi-arid and arid areas. Recently, dew and fog water harvesting has been introduced in semi-arid areas as a source of water [3–11].

The atmospheric contains huge amounts of water vapor that can be harvested and used as an alternative freshwater supply [12]. According to the typical picture of the Earth's hydrologic cycle, water is continuously re-circulated and transported between oceans, land, and atmosphere. Besides vertical convection of water vapor and cloud formation, water vapor might transport nearby the Earth's surface and end up with forming fog, smog, and mist as well as the condensation on cooled surfaces (i.e., dew formation). Dew and fog formation a very complex phenomenon that involves water vapor condensation on a substrate (e.g., environmental surfaces) or on an airborne particle (e.g., forming fog) [13–19]. It has been understood as a two-step process: (1) formation of droplets on obstacles (particle, surface, etc.) via nucleation of water vapor and (2) droplet growth due to condensation of water vapor [18]. Thermodynamically, dew is a phase transition from the vapor phase into the liquid/solid phase on a substrate held at a lower temperature than that of the gas. As postulated by Beysens [19], the presence of a substrate that geometrically constrains the growth is the origin of the peculiarities and richness of the phenomenon. A key point is the droplet interaction through droplet fusion or coalescence, which leads to scaling in the growth and gives universality to the process. Usually, dew formation occurs overnight.

The attention about dew formation has been given to the amount harvested and the quality of harvested water (e.g., potable water or utilized in for other applications) [20–32]. Several groups have developed different methods and tools to harvest dew in different environments [6,19,20,28,33–41]. The most common experimental methods included passive condensers, radiative cooling, roofs (made of different materials, and surfaces made a material that enhances the yield of dew. The condensers are made of suitable materials and are thermally isolated from the ground. As an empirical result, it is possible to increase the amount of harvested dew water by utilizing the most suitable method [9–27]. However, sustainable and long-term experimental studies about dew formation seem to be almost impossible. As such, the potential of dew yield has been investigated using model simulation (kindly see the review study by Tomaszkiewicz et al. [42]). The simplest and most applicable models are those based on the semi-empirical approaches implementing heat-mass transfer and energy balance [8,14,15,41–49]. Some of these models were developed for a regional and global scale [41,44,48]. The same principle was also applied for specific environments [4,45,47,50,51].

Recently, there have been only two investigations about dew water in Jordan, which is a semi-arid region with an average annual rainfall of less than 120 mm in most desert areas and 300–600 mm in the mountain heights [24,27]. The first one reported some elemental and ions concentrations in dew water [24]. Odeh et al. [27] collected 15 samples of dew water on a substrate (during March–July 2015) in an urban area in Amman and reported the collected amount and quality by applying chemical and physical analysis. In practice, harvested dew water in Jordan may not be potable but it can be useful for agriculture purposes. However, dew formation yield has never been assessed theoretically in Jordan.

In this study, we performed model simulations to estimate the dew yield during 40 years (1979–2018) in Jordan. The model simulations were made by adapting the global model, which was developed by Vuollekoski et al. [41], to accommodate the environmental conditions at ten locations selected in different environments in Jordan. The model simulations were performed for selected 10 locations, which represented the different climate zones in Jordan. The ultimate goal was to investigate the spatio-temporal variation of dew formation during a long-term period. The outcomes of this study are ought to be useful for managing and planning local feasibility studies for dew harvesting. The long-term model simulation output can be also utilized to understand the feedback processes between the water cycle and climate change in Jordan.

2. Materials and Methods

2.1. Modeling of Dew Formation

We utilized a modified version of the global dew formation model to simulate the dew formation yield at ten selected locations in Jordan (Figure 1, Table 1). The detailed model description is presented in

Appendix A. The model simulations covered a long-term period from 1979–2018 (40 years). The selected locations represented different environments: urban, mountains, desert, coastal, and valley.

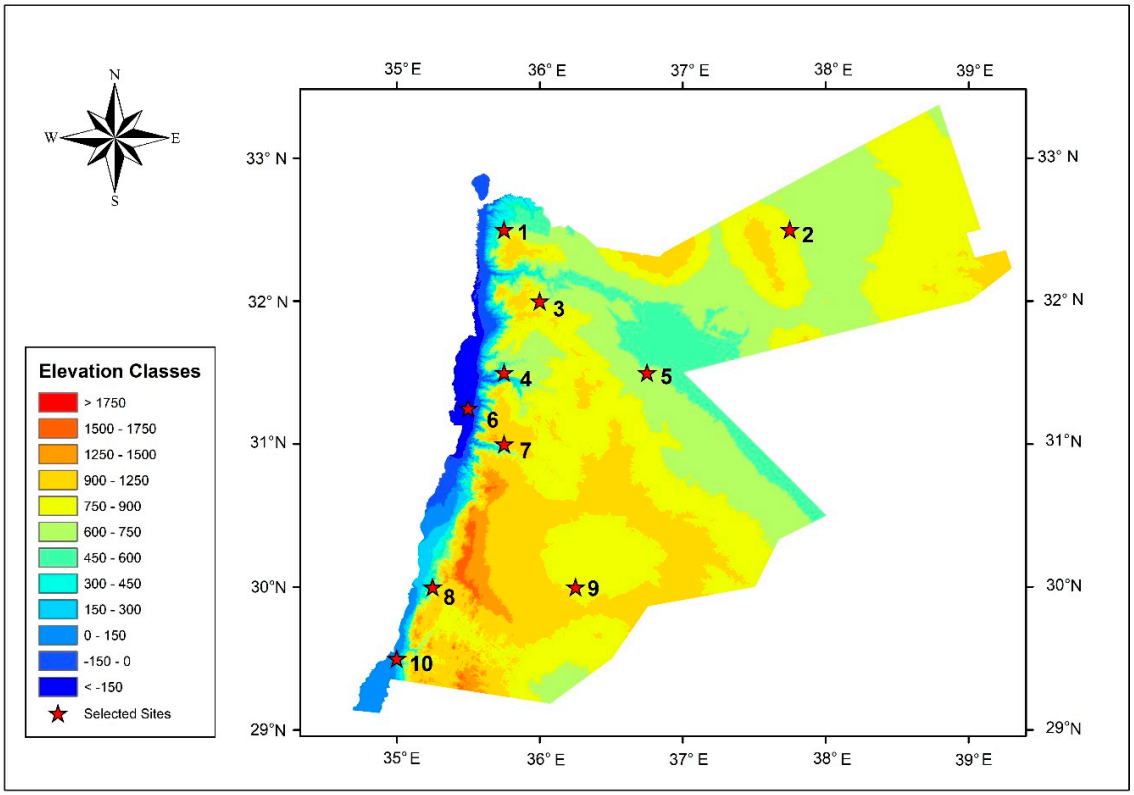

Figure 1. A map of Jordan illustrating the geographical topography and the selected location, where the model simulation was performed. See also Table 1 for locations characteristics.

Table 1. Selected locations and their geographical and environmental characteristics.

Station Number	Elevation (m.a.s.l)	Region and Area Type	Location	T_a (°C) Mean (Min–Max)	DP (°C)	RH %	Dew Yield (mm/y)
1	530	Mountain, agriculture	Irbid	18 (11–24)	10 (8–13)	66 (40–84)	89
2	780	Arid, rural	Mafraq	19 (12–26)	4 (0–7)	43 (25–60)	21
3	730	Mountain, urban	Amman	19 (12–25)	9 (6–12)	60 (34–81)	56
4	720	Mountain, agriculture	Madaba	20 (13–26)	9 (6–12)	58 (33–79)	58
5	630	Badia, rural	Azraq	20 (13–26)	6 (2–9)	49 (27–68)	23
6	−400	Valley, agriculture	Dead Sea	20 (13–26)	9 (6–12)	58 (32–79)	63
7	790	Mountain, agriculture	Karak	19 (12–26)	8 (4–11)	55 (29–76)	47
8	770	Mountain, Arid	Petra	20 (12–27)	7 (3–10)	49 (26–70)	42
9	890	Badia, rural	Ma'an	20 (12–27)	4 (0–8)	43 (22–62)	20
10	110	Costal, arid	Aqaba	20 (13–27)	6 (2–9)	48 (25–68)	29

2.2. Case Study Description—Jordan

2.2.1. Climate Types

Jordan is a small country (~89,000 km^2, population ~10 million in 2016). It is located (29°–34° North and 34°–40° East) at the Asian–African continental border-line and about 100 km east of the Mediterranean Sea. It has diverse habitats, ecosystems, biota due to its varied landscapes, environments, and climates.

The summer season in Jordan is hot-dry and spans from May to September with a mean temperature of ~32 °C (sometimes exceeds 40 °C in July and August). The winter is relatively cool and

spans from November to March with mean temperature ~13 °C and frequent showers and occasional snowfall in some elevated areas.

Geographically, Jordan comprises a wide variety of topography that defines its climate spatial variation [52,53]. There are three distinguished climatic zones in Jordan: (1) *Jordan Valley*, (3) the *Eastern Desert* (also known as *Badia*), and (3) *Mountains Heights Plateau*. The *Jordan Valley* (including Jordan River and the Dead Sea) climate ranges from arid to semi-arid with a hot dry summer, warm winter, and precipitation less than 200 mm/yr. The climate in the *Badia* is characterized by a sharp change in temperature between day and night and between summer and winter. For example, the daytime summer temperature in *Badia* can exceed 40 °C and the winter nights can be very cold, dry, and windy. Precipitation in *Badia* is less than 100 mm/year.

The *Mountains Heights Plateau* (including highlands above the Jordan Valley, mountains of the Dead Sea, Wadi Araba, and Ras Al-Naqab) are mainly situated in the western region starting at the northern part parallel to the *Jordan Valley* and extended to the south approaching Wadi Rum and Aqaba. The climate on the *Mountains Heights Plateau* is a typical Mediterranean climate with a hot-dry summer and cool-wet winter with two short transitional seasons. The *Mountains Heights Plateau* receives Jordan's highest amounts of precipitation (more than 300 mm/year), which falls during October–May with the peak usually during winter (December–February).

2.2.2. Fresh Water Resources

Jordan is the fourth country in the world suffering from freshwater shortages. The main sources of water in Jordan include safe abstraction of groundwater, recycling wastewater, surface runoff water, and desalination. The annual mean water amount received in the form of rainfall is about 8300 million cubic meters (MCM) [54]. The available water per capita has declined considerably during the past century; it was about 3600 m^3 in 1946 and it is expected to be as low as 100 m^3 in 2025 [55]. Jordan's water demand estimated to be about 940 MCM (63% agriculture, 32% domestic, and 5% industry) in 2007 and it increased to be about 1600 MCM in 2010. Groundwater capacity consists of twelve identified basins with the critical state due to maximum capacity exploitation. The Jordanian authorities have built ten water dams to utilize the stored water and satisfy livestock needs and groundwater recharge [55]. In addition, surface water has a share of about 28% of the total water supply in the country.

3. Results

3.1. Spatial Variation of the Cumulative Dew Yield

We calculated the overall average cumulative yield of dew in liquid form (i.e., condensation as liquid water) and solid form (Table 2). The conditions to calculate dew in the solid phase (i.e., hoarfrost) were described in detail in the methods section. In brief, this happens when $T_c < 0$ °C. This condition was rarely valid almost for all sites (i.e., less than 1 mm). The only exception was in Mafraq, where the mean hoarfrost yield was ~2 ± 1 mm.

The highest overall average water dew yield was obtained for the site on the *Mountains Heights Plateau*, which has a Mediterranean climate. At these sites, the overall average water dew yield was 46 ± 6, 40 ± 6, 55 ± 6, 57 ± 6, and 88 ± 7 mm, respectively, for Petra (site 8), Karak (Site 7), Amman (Site 3), Madaba (Site 4), and Irbid (Site 1). These regions have a Mediterranean climate with humid winter and hot dry summer. Average air temperature, dew point temperature, and relative humidity in these sites are 19 °C, 9 °C, and 58%; respectively (Table 1). The lowest overall average water dew yield was obtained for the sites located in the *Badia* had the least overall average water dew yield: Ma'an (site 9, 19 ± 3 mm), Mafraq (site 2, 19 ± 4 mm), and Azraq (site 5, 22 ± 4 mm). All these sites were located in the *Eastern Desert* climate (also known as *Badia*).

The Dead Sea (site 6) also was one of the sites that showed a high value for the overall average water dew yield (about 63 ± 7 mm). Aqaba (site 10) had an overall average water dew yield of about 28 ± 3 mm. From a climatological point of view, the Aqaba site is affected by the desert climate.

Table 2. Overall mean ± standard deviation as well as the range of the yearly cumulative dew yield. The values are listed as mean ± Std (min–max) in mm.

Site Number	Site Name	Water	Hoarfrost	Water + Hoarfrost
1	Irbid	88 ± 7 (75–104)	1 ± 0.8 (0–3)	89 ± 6 (75–105)
2	Mafraq	19 ± 4 (11–30)	2 ± 1 (0–4)	21 ± 4 (12–30)
3	Amman	55 ± 6 (41–65)	1 ± 0.7 (0–3)	56 ± 6 (42–66)
4	Madaba	57 ± 6 (42–67)	1 ± 0.7 (0–2.5)	58 ± 6 (43–67)
5	Azraq	22 ± 4 (14–29)	1 ± 0.6 (0–2.5)	23 ± 4 (15–29)
6	Dead Sea	63 ± 7 (46–73)	1 ± 0.5 (0–2)	63 ± 7 (46–74)
7	Karak	46 ± 6 (33–56)	1 ± 0.7 (0–3)	47 ± 6 (33–57)
8	Perta	40 ± 6 (29–52)	1 ± 0.7 (0–3)	42 ± 6 (30–53)
9	Ma'an	19 ± 3 (12–26)	1 ± 0.8 (0–4)	20 ± 3 (13–27)
10	Aqaba	28 ± 5 (18–38)	1 ± 0.6 (0–3)	29 ± 5 (19–39)

3.2. Temporal Variation of the Cumulative Dew Yield

During the past two decades, dew yield has declined at all sites, especially in the arid and semi-arid sites (Figures 2 and 3). It is not surprising to see the model predicted such a decline during that period because the climate change impacts were very pronounced by increased desertification and potential of sand and dust storms (SDS) in the region [56,57] as will be discussed later.

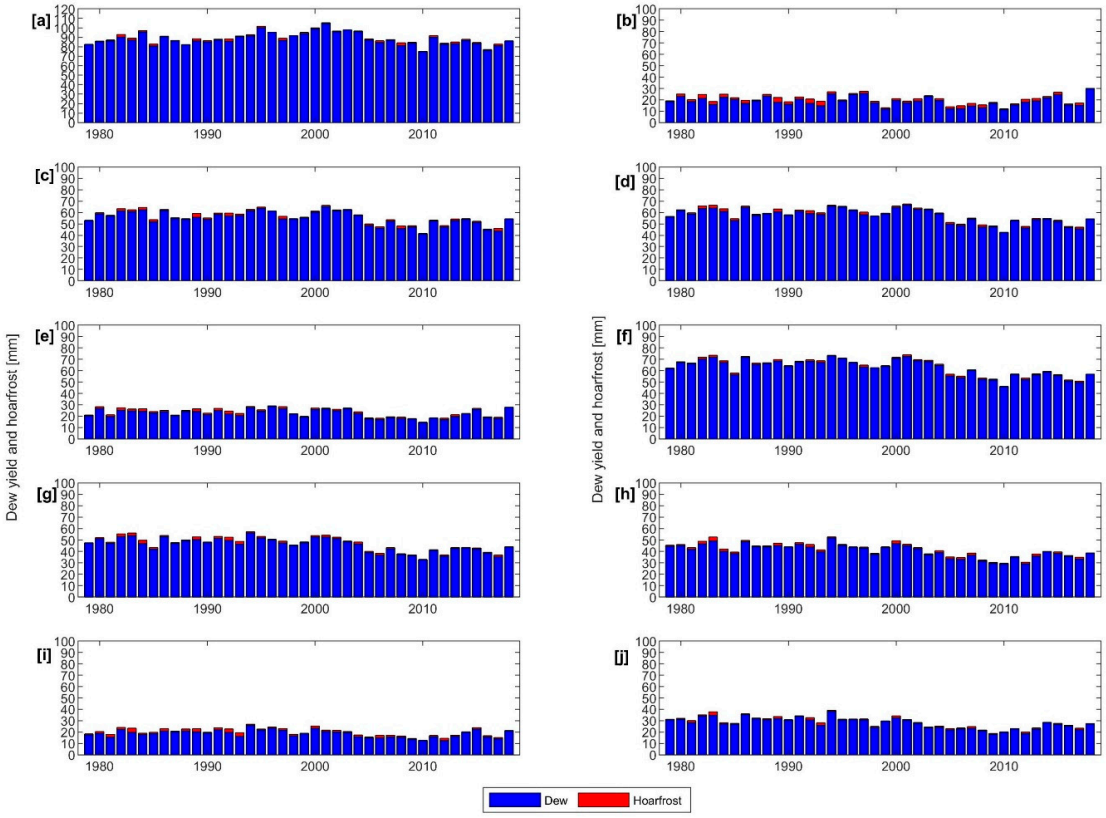

Figure 2. Yearly cumulative dew yield and ice (i.e., hoarfrost) during 1979–2018 at the selected sites: (**a**) Irbid, (**b**) Mafraq, (**c**) Amman, (**d**) Madaba, (**e**) Azraq, (**f**) Dead Sea, (**g**) Karak, (**h**) Petra, (**i**) Ma'an, (**j**) Aqaba. The subplots are in sequential order according to site number from 1 to 10 (Figure 1).

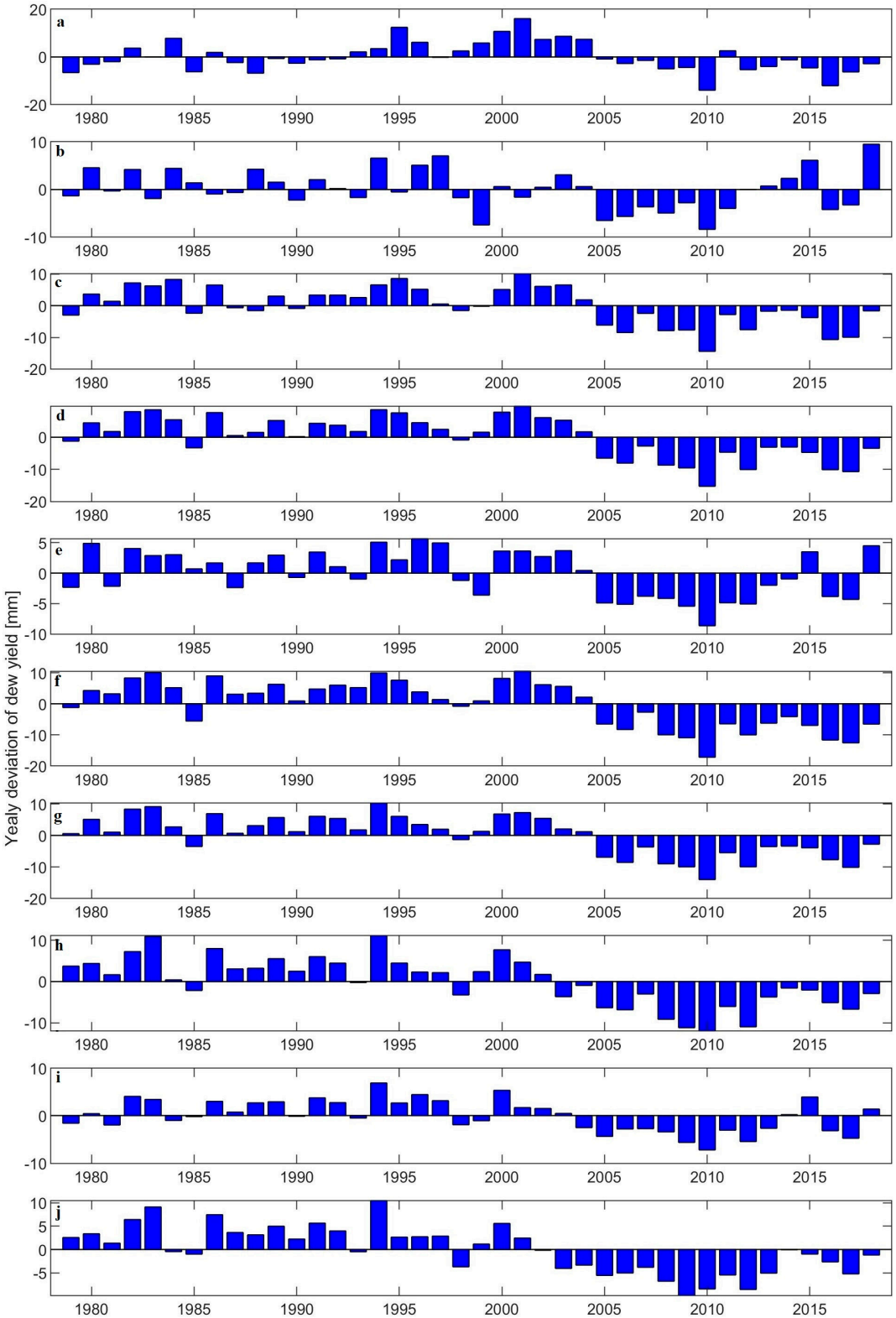

Figure 3. Difference between mean yearly dew yield and yearly long term mean during 1979–2018 at the selected sites: (**a**) Irbid, (**b**) Mafraq, (**c**) Amman, (**d**) Madaba, (**e**) Azraq, (**f**) the Dead Sea, (**g**) Karak, (**h**) Petra, (**i**) Ma'an, (**j**) Aqaba. The subplots are in sequential order according to site number from 1 to 10 (Figure 1).

The Mann–Kendal trend analysis [58] at confidence level 95% ($p < 0.05$) revealed a significant negative trend for the yearly mean dew yield at all selected sites (Table 3). To find out the reason for such a decreasing trend in dew yield, we investigated the trend analysis results for air temperature, dew point temperature, and relative humidity. These are key factors in dew formation. Air temperature (T_a, $T_{max,}$ and T_{min}) and relative humidity showed a significant positive and negative trend during the 40 years (Tables 4 and 5). T_d did not show any significant trend. Nevertheless, it seems that the negative trend in dew yield was a result of the increase in temperature and decrease in relative humidity in the past 40 years.

Table 3. Mann–Kendal trend test predicted by Sen's slope estimator for yearly mean dew yield during 1979–2018.

Site Number	Site Name	Slope (Per Year)	Slope (Per Decade)
1	Irbid	−0.08	−0.8
2	Mafraq	−0.07	−0.7
3	Amman	−0.2 *	−2
4	Madaba	−0.3 *	−3
5	Azraq	−0.1 *	−1
6	Dead Sea	−0.4 *	−4
7	Karak	−0.3 *	−3
8	Perta	−0.3 *	−3
9	Ma'an	−0.1 *	−1

* Values with a star indicate a statistically significant trend with $p < 0.05$.

Table 4. Mann–Kendal trend test predicted by Sen's slope estimator for yearly mean air temperature during 1979–2018.

Site Number	Site Name	Slope	R^2	Slope (Min)	Slope (Max)
1	Irbid	0.04 *	0.52	0.03 *	0.4 *
2	Mafraq	0.04 *	0.39	0.03 *	0.3 *
3	Amman	0.04 *	0.55	0.03 *	0.4 *
4	Madaba	0.04 *	0.57	0.03 *	0.5 *
5	Azraq	0.04 *	0.5	0.03 *	0.4 *
6	Dead Sea	0.04 *	0.59	0.4 *	0.5 *
7	Karak	0.04 *	0.57	0.03 *	0.5 *
8	Perta	0.04 *	0.57	0.03 *	0.4 *
9	Ma'an	0.04 *	0.5	0.03 *	0.4 *
10	Aqaba	0.04 *	0.58	0.04 *	0.4 *

* Values with a star indicate a statistically significant trend with $p < 0.05$.

Table 5. Mann–Kendal trend test predicted by Sen's slope estimator for yearly mean relative humidity during 1979–2018.

Site Number	Site Name	Slope (per Year)	Slope (per Decade)	R^2
1	Irbid	−0.1 *	−1	0.57
2	Mafraq	−0.09 *	−0.9	0.16
3	Amman	−0.2 *	−2	0.6
4	Madaba	−0.1 *	−1	0.47
5	Azraq	−0.2 *	−2	0.66
6	Dead Sea	−0.2 *	−2	0.66
7	Karak	−0.1 *	−1	0.59
8	Perta	−0.1 *	−1	0.44
9	Ma'an	−0.09 *	−0.9	0.31
10	Aqaba	−0.1 *	−1	0.39

* Values with a star indicate a statistically significant trend with $p < 0.05$.

There were three seasonal patterns of dew yield (Figures 4 and 5):

- Pattern-I: high values (exceeding 100 mL/m^2) for the daily cumulative dew yield during the cold period of the year (November–March) and very minimal (almost vanishing) dew during the warm period of the year (June–August).
- Pattern-II: considerable amounts of daily cumulative dew yield exceeding 100 mL/m^2 throughout the year with values exceeding 200 mL/m^2 during the winter (December–February).
- Pattern-III: rather constant daily cumulative dew yield (about 200 mL/m^2) during the winter and spring (December–May) and increased values during the summer and autumn (namely peak value ~350 mL/m^2 in August).

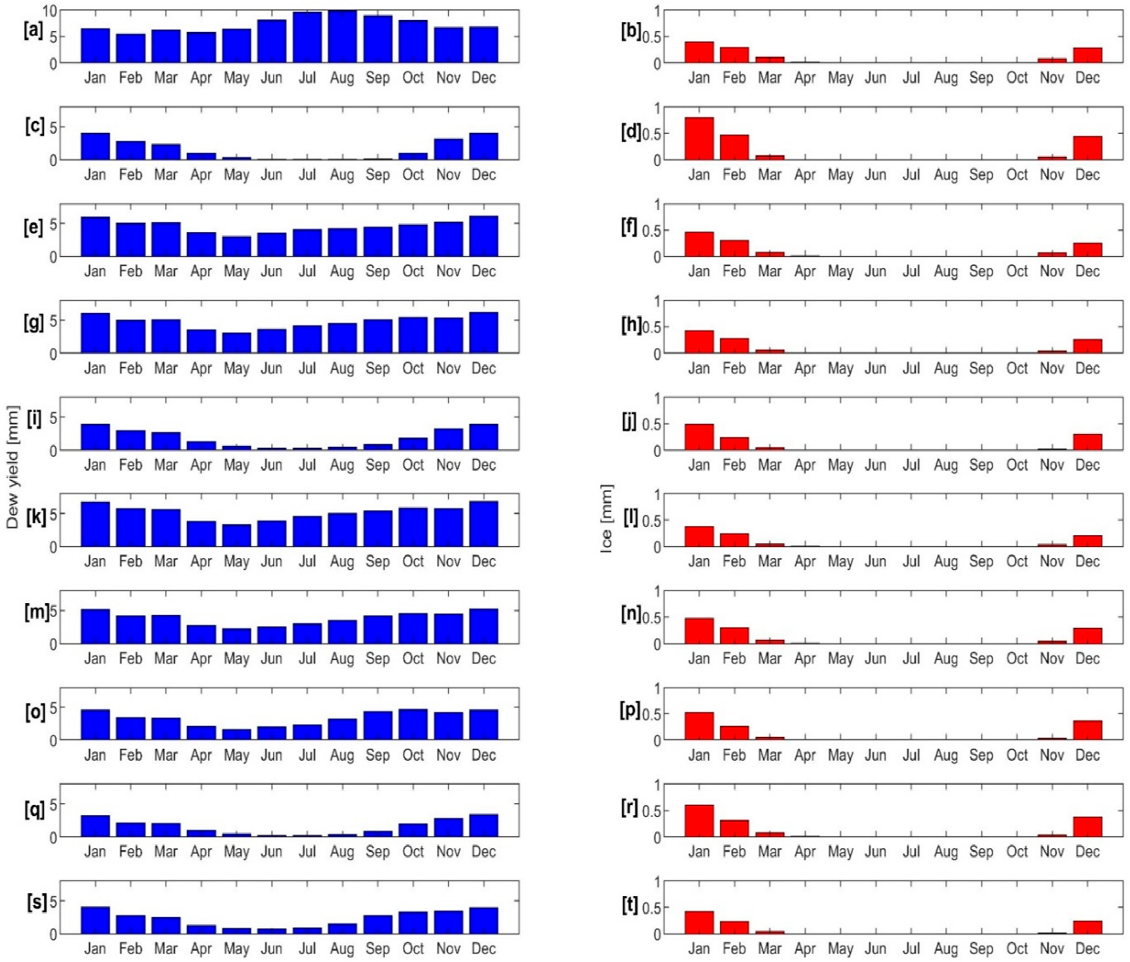

Figure 4. Mean monthly cumulative dew yield (left panel) and ice (i.e., hoarfrost) (right panel) at the selected sites during 1979–2018: (**a**,**b**) Irbid, (**c**,**d**) Mafraq, (**e**,**f**) Amman, (**g**,**h**) Madaba, (**i**,**j**) Azraq, (**k**,**l**) Dead Sea, (**m**,**n**) Karak, (**o**,**p**) Petra, (**q**,**r**) Ma'an, (**s**,**t**) Aqaba. The subplots are in sequential order according to site number from 1 to 10 (Figure 1).

Again, these patterns reflected the three distinguished climate zones in Jordan. For example, Pattern-I was seen for Mafraq (site 2), Azraq (site 5), Ma'an (site 9), and also Aqaba (site 10); these sites are all within the arid climate in the *Badia* zone. Pattern-II was mainly seen for Amman (site 3), Madaba (site 4), Karak (site 7), and Petra (site 8); all are within the Mediterranean climate zone on *Mountains Heights Plateau*. Although the Dead Sea (site 6) is located within the semi-arid climate zone (*Jordan Valley*), but it showed a similar seasonal pattern as that seen for the sites on the *Mountains Heights Plateau*. Even though Irbid (site 1) is a site with a Mediterranean climate as it is located on the *Mountains Heights Plateau* zone, but it had a very distinguished seasonal pattern (i.e., Pattern-III),

which had elevated values of dew yield during the summer and autumn. This is not surprising because Irbid (site 1) is also located at the edge of the Fertile Crescent, which receives the highest amounts of rainfall and it seems to be a site favoring dew formation as well.

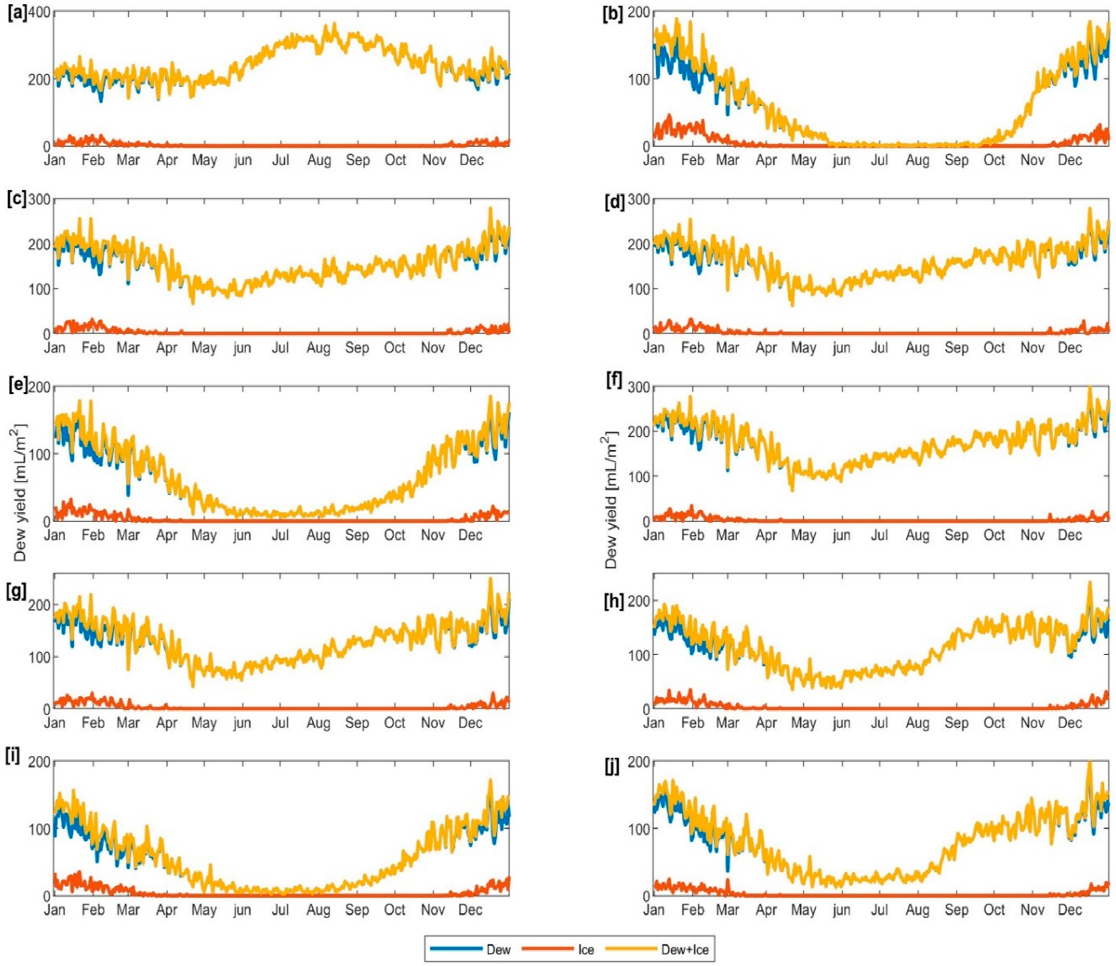

Figure 5. Mean daily cumulative dew yield (blue line), ice (i.e., hoarfrost) (red line) and dew + ice (yellow line) during 1979–2018 at the selected sites: (**a**) Irbid, (**b**) Mafraq, (**c**) Amman, (**d**) Madaba, (**e**) Azraq, (**f**) Dead Sea, (**g**) Karak, (**h**) Petra, (**i**) Ma'an, (**j**) Aqaba. The subplots are in sequential order according to site number from 1 to 10 (Figure 1).

4. Discussion

The difference in the dew formation yield among selected sites reflected the climate variation described before in the methods section; i.e., *Jordan Valley* zone (site 6), *Eastern Desert* (also known as *Badia*) zone (sites 2, 5, and 9), and *Mountains Heights Plateau* zone (sites 1, 3, 4, 7, and 8). Aqaba (site 10) was a coastal site, but it was not one of the sites with high overall average dew yield due to its location very close to the arid and desert region; the higher the temperature is the higher potential to keep the water vapor in the gas phase and that prevents condensation on surfaces (i.e., dew formation).

As for the dew yield decline during the past two decades (2005–2018) and the climate change impacts, two previous studies reported increased desertification and potential of sand and dust storms (SDS) in the Middle region due to warming and drying episodes [56,57]. For example, warming and drying episodes increased during that period [56]. In turn, these have significant impacts on the albedo and short-wave radiation leading to higher surface reflection [59], which directly affects the potential of dew formation. Besides climate change impacts, the increased emissions of anthropogenic air pollution impact the potential of dew formation [60] because submicron particles slow down the conversion

of water vapor from the gas phase to the liquid phase. This, in turn, escalated the desertification process in the Middle East causing increased frequency of dust episodes and atmospheric dust particles concentrations, which affected the albedo and the short-wave radiation as per the discussion above. The processes involved in dew formation can be similar to that involved in the cloud droplet formation with a difference that clouds are formed on by condensation on supercooled particles (i.e., cloud condensation nuclei CCN) whereas dew is formed by condensation on environmental surfaces with their temperature lower than the dew point. Therefore, anthropogenic air pollution might also similarly hinder dew formation.

To have an insight into seasonal patterns of dew yield, we investigated the long-term mean of the seasonal variation for some meteorological parameters (T_a, T_d, RH, WS, surface pressure, and total cloud cover), which are key factors in dew formation (Figures S1–S10 in Supplementary Material). Regardless of the variation in the amount of dew yield, the peak of dew formation can occur in the wintertime (November–February). Indeed, during the cold season, temperature declines in all parts of Jordan (mean T_a ~ 10 °C). Besides that, the domination of the prevailing westerly winds brings humid air from the Mediterranean Sea into the country; consequently, the relative humidity rises, and the difference between the temperature and the dew point (T_a–T_d) decreases. All these together with the increasing cloud cover, which is a result of the Mediterranean cyclones, provide the initial conditions for dew formation in the winter. Therefore, dew occurs frequently in most parts of Jordan during the wintertime.

Differences in the amount of dew yield are clear in different locations (~100–350 mL/m^2). Although the probability of dew occurrence in winter is mainly similar at all sites, but it is different in summer. In fact, the occurrence of dew in winter is mostly controlled by synoptic conditions whereas in summer it is more dependent on local conditions and is largely affected by the features of the climate zones. For instance, in Mafraq (site 2), Azraq (site 5), Ma'an (site 9), and Aqaba (site 10), which all were within the arid climate in the *Badia* zone, dew is almost vanished during late spring and summer (May–September). Indeed, in the summer, the temperature sometimes exceeds 40 °C (especially in July and August), and relative humidity is very low, the sky is often clear, the daytime duration is long, and the incoming short-wave radiation exceeds the outgoing long wave radiation. Furthermore, high surface temperature leads to form thermal low-pressure system, which cause turbulence and an intense wind speed. As such, condensation cannot occur, and dew is almost vanished during the warm season.

Dew occurred throughout the year in Amman (site 3), Madaba (site 4), Karak (site 7), and Petra (site 8) as a result of the moist air fronts prevailing from the Mediterranean Sea (i.e., sea breeze, especially after sunset). However, the Mediterranean Sea breeze does not reach beyond 100 km inland. Furthermore, these sites were located on high elevation; thus, the temperature drops in the night and T_a–T_d is reduced, which favors dew formation.

An interesting result was observed in Irbid (site 1). This site had a unique seasonal pattern of dew formation with a significant potential for dew formation throughout the year (~90 mm/year) and a maximum daily dew yield during summer and early autumn (July–September). This site has close surface water in the north (i.e., the Sea of Galilee) and receives the Mediterranean Sea breeze more efficiently than any other region in Jordan. The temperature is also moderate in this region during the summer, which another reason that favors dew formation in the summer. One reason for higher dew yield in summer than winter in this site could be due to air temperature. On the other hand, in wintertime due to lower temperatures, the atmosphere cannot keep a significant amount of moisture, whereas during warm season with a rise in temperature, the atmospheric capacity to keep water vapor increases. This means that high capacity of moisture can compensate for high temperatures in summer and lower T_a–T_d. All these conditions together with light wind speed (i.e., less than 2 m/s) stimulate dew formation in Irbid during the summer.

5. Conclusions

Water resources are very scarce in Jordan. There is a great need to look for additional water resources; and hence, dew can be one of such potential sources to be utilized for agricultural purposes. In this study, we performed model simulations to investigate the spatial, seasonal, and annual dew yield during 40 years (1979–2018). We considered ten locations selected in different geographical locations but have the same altitude to reflect the variation of climate and environmental conditions.

In accordance with the climate zones in Jordan, the dew yield had distinguished characteristics features with respect to the yield, seasonal variation, and spatial variation. The highest water dew yield was obtained for the *Mountains Heights Plateau*, which has a Mediterranean climate, with an overall annual average water dew yield was as high as 88 mm. The *Badia*, which has an arid climate, received the least dew yield with an overall annual average water dew yield was as low as 19 mm. During the past two decades, the dew yield was declined as a result of climate change impacts in the form of increased desertification and the potential of sand and dust storms (SDS) in the region. In addition, the increased anthropogenic air pollution impacted the potential of dew formation because submicron particles slow down the conversion of water vapor condensation on obstacles.

According to the model simulations, each climate zone in Jordan had a distinguished dew yield seasonal pattern. The first pattern was characterized by high yield value (daily cumulative exceeding 100 mL/m^2) during winter and almost vanishing yield during summer. The second pattern is characterized by significant amounts of daily cumulative dew yield (exceeding 100 mL/m^2) throughout the year with yields as high as 200 mL/m^2 during the winter. The third pattern was characterized by a rather constant daily cumulative dew yield (about 200 mL/m^2) during the winter and spring and high yield values (as high as 350 mL/m^2) during the summer and autumn.

The outcome of this research can be utilized for managing and planning local feasibility studies for dew harvesting in Jordan. Knowing the locations with the highest dew formation potential is important from a strategic point of view to make the suitable decision for commissioning dew water harvesting as a secondary source of water to be used in different sectors. In the future, model calibration is the most important part is validating the results in this study and carry it beyond selected locations and cover all parts of Jordan (i.e., gridded model simulation). Model validation requires long-term dew harvesting in different locations, which is laborious. The upcoming research in this context is to prepare for the long-term measurement campaign and redo the model simulation for a gridded domain covering whole Jordan.

Supplementary Materials: The following are available online at http://www.mdpi.com/2073-4441/12/8/2186/s1, Figure S1: Long-term mean seasonal variation of (**a**) air temperature (point blue line), dewpoint temperature (solid blue line), relative humidity (red line), (**b**) wind speed at 2 m height (blue line) and surface pressure (red line) and (**c**) total cloud cover (blue line) in Irbid (site 1), Figure S2: Long-term mean seasonal variation of (**a**) air temperature (point blue line), dewpoint temperature (solid blue line), relative humidity (red line), (**b**) wind speed at 2 m height (blue line) and surface pressure (red line) and (**c**) total cloud cover (blue line) in Mafraq (site 2), Figure S3: Long-term mean seasonal variation of (**a**) air temperature (point blue line), dewpoint temperature (solid blue line), relative humidity (red line), (**b**) wind speed at 2 m height (blue line) and surface pressure (red line) and (**c**) total cloud cover (blue line) in Amman (site 3), Figure S4: Long-term mean seasonal variation of (**a**) air temperature (point blue line), dewpoint temperature (solid blue line), relative humidity (red line), (**b**) wind speed at 2 m height (blue line) and surface pressure (red line) and (**c**) total cloud cover (blue line) in Madaba (site 4), Figure S5: Long-term mean seasonal variation of (**a**) air temperature (point blue line), dewpoint temperature (solid blue line), relative humidity (red line), (**b**) wind speed at 2 m height (blue line) and surface pressure (red line) and (**c**) total cloud cover (blue line) in Azraq (site 5), Figure S6: Long-term mean seasonal variation of (**a**) air temperature (point blue line), dewpoint temperature (solid blue line), relative humidity (red line), (**b**) wind speed at 2 m height (blue line) and surface pressure (red line) and (**c**) total cloud cover (blue line) in Dead Sea (site 6), Figure S7: Long-term mean seasonal variation of (**a**) air temperature (point blue line), dewpoint temperature (solid blue line), relative humidity (red line), (**b**) wind speed at 2 m height (blue line) and surface pressure (red line) and (**c**) total cloud cover (blue line) in Karak (site 7), Figure S8: Long-term mean seasonal variation of (**a**) air temperature (point blue line), dewpoint temperature (solid blue line), relative humidity (red line), (**b**) wind speed at 2 m height (blue line) and surface pressure (red line) and (**c**) total cloud cover (blue line) in Petra (site 8), Figure S9: Long-term mean seasonal variation of (**a**) air temperature (point blue line), dewpoint temperature (solid blue line), relative humidity (red line), (**b**) wind speed at 2 m height (blue line) and surface pressure (red line) and (**c**) total cloud cover (blue line) in Ma'an (site 9), Figure S10: Long-term mean seasonal variation of (**a**) air

temperature (point blue line), dewpoint temperature (solid blue line), relative humidity (red line), (**b**) wind speed at 2 m height (blue line) and surface pressure (red line) and (**c**) total cloud cover (blue line) in Aqaba (site 10).

Author Contributions: Conceptualization, D.R., T.H., and N.A.; methodology, H.V. and N.A.; validation, N.A. and T.H.; formal analysis, N.A. and T.H.; Software, N.A. and H.V.; investigation, N.A.; resources, T.V. and M.K.; data curation, N.A.; writing-original draft preparation, N.A. and T.H.; writing-review and editing, N.A., T.H., D.R. M.A.K., J.A., M.K., and T.V.; visualization, N.A. and T.H.; supervision, D.R., T.H., and T.V.; project administration, D.R., T.H., and T.V. All authors have read and agreed to the published version of the manuscript.

Funding: Open access funding provided by the University of Helsinki.

Acknowledgments: The University of Isfahan is acknowledged to facilitate the research visit abroad for graduate students. The Ministry of Science, Research, and Technology supported Nahid Atashi to visit the University of Helsinki, Institute for Atmospheric and Earth System Research (UHEL-INAR). The University of Helsinki hosted Atashi twenty months of her research visit working on dew yield potential modeling. This visit was also under the Academy of Finland Center of Excellence programme (CoE-ATM, grant no. 307331) and Academy Professor projects (312571 and 282842). This manuscript was written and completed during the sabbatical leave of the last author (Tareq Hussein) that was spent at the University of Helsinki and supported by the University of Jordan during 2019.

Conflicts of Interest: The authors declare no conflict of interest.

Appendix A

Appendix A.1. Model Description

The global dew formation model, which was developed by Vuollekoski et al. [41], was modified to accommodate for environmental conditions in Jordan. The original model setup was made suitable for a global contest and can handle water phase change between vapor and liquid or solid (i.e., condensation and desublimation); only dew was considered but precipitation and fog were not. The substrate (i.e., condenser material) was assumed a horizontally aligned sheet (at 2 m height and thermally insulated from the ground) of a suitable material such as low-density polyethylene (LDPE) or polymethylmethacrylate (PMMA).

The model describes the water phase change based on mass and heat balance Equation

$$\frac{dT_c}{dt}(C_c m_c + C_w m_w + C_i m_i) = P_{rad} + P_{cond} + P_{conv} + P_{lat} \quad \text{(A1)}$$

where dT_c/dt is the change rate in the condenser temperature. C_c, C_w, and C_i are the specific heat capacity of condenser, water, and ice; respectively. Here, m_c, m_w, and m_i are mass of condenser, water, and ice; respectively. The right-hand side describes the heat exchange involved in the heat exchange processes: P_{rad} is the incoming and outgoing radiation, P_{cond} is the conductive heat exchange between the condenser surface and the ground, P_{conv} is the convective heat exchange, and P_{lat} is the latent heat released by the condensation or desublimation of water. The model reads all input data for a given grid point and solves equations. using a fourth-order Runge–Kutta algorithm with a 10 s time step. All terms in Equation (A1) are described in more detail in Tables A1 and A2.

The model was set up so that it assumes similar conditions for the phase-change of pre-existing water or ice on the condenser sheet. For instance, if the water on the condenser is in the liquid phase (i.e., $m_w > 0$) and the condenser temperature $T_c < 0$ °C, then the sheet is losing energy (i.e., the right-hand side of Equation (A1) is negative). In that case, instead of solving Equation (A1), Tc is assumed constant and the lost mass from the liquid phase of water is transferred to the cumulated mass of ice; i.e., the water is transformed from liquid phase to solid phase. Consequently, Equation (A1) is replaced by

$$L_{wi}\frac{dm_w}{dt} = P_{rad} + P_{conv} + P_{lat}, \quad \text{(A2)}$$

where L_{wi} [J kg^{-1}] is the latent heat of fusion. If the water on the condenser is in the solid phase (i.e., $m_i > 0$) and the condenser temperature $T_c > 0$ °C, a similar equation is assumed for the change rate of ice mass (m_i).

Note that Equation (A2) is not related to the condensation of water; it only describes the phase change of the already condensed water or ice on the condenser. For the water condensation rate, which is assumed independent of Equation (A2), the mass-balance equation is then assumed to be

$$\frac{dm}{dt} = \max[\,0\,,\; S_c k(\,P_{sat}(T_d) - P_c(T_c)\,)\,], \tag{A3}$$

where m represents either the mass of ice (m_i) or water (m_w) depending on weather Tc is below or above 0 °C. $P_\mathrm{sat}(T_\mathrm{d})$ is the saturation pressure at the dew point temperature whereas $P_\mathrm{c}(T_\mathrm{c})$ is the vapor pressure over the condenser sheet. k = h/L_vw $\gamma = 0.622\ h/C_\mathrm{a}\ p$ is the mass transfer coefficient, where L_vw [J kg^{-1}] is the specific latent heat of water vaporization, γ is the psychrometric constant, C_a is the specific heat capacity of air, and p is the atmospheric air pressure. Here, h = 5.9 + 4.1 u (511 + 294)/(511+T_a) is the heat transfer coefficient, where u and Ta are the prevailing horizontal wind speed and the ambient temperature at 2 m from the ground.

Table A1. Description of the dew formation model by listing the terms in Equation (A1).

Term	Unit	Description
dT_c/dt	K s^{-1}	Change rate of the condenser temperature
T_c	K	Temperature of the condenser
T	s	Time. Here the time step in the model was 10 s
C_c	J kg^{-1} K^{-1}	Specific heat capacity of the condenser. For low-density polyethylene (LDPE) and polymethylmethacrylate (PMMA) it is 2300 J kg^{-1} k^{-1}
C_i	J kg^{-1} K^{-1}	Specific heat capacity of ice (2110 J kg^{-1} k^{-1})
C_w	J kg^{-1} K^{-1}	Specific heat capacity of water (4181.3 J kg^{-1} k^{-1})
m_c	kg	Mass of the condenser given by $m_c = \rho_c S_c \delta_c$ where ρ_c, S_c, and δ_c are the density (here it is 920 kg m^{-3}), surface area (here it is 1 m^2), and thickness of the condenser (here it is 0.39 mm)
m_i	kg	Mass of ice
m_v	kg	Mass of water, representing the cumulative mass of water that has
P_{rad}	W	Heat exchange due to incoming and outgoing radiation $P_{rad} = (1-a)S_c R_{sw} + \varepsilon_c S_c R_{lw} - S_c \varepsilon_c \sigma {T_c}^4$ where a is the condenser short-wave albedo (here it is 0.84), S_c is the condenser surface area (here it is 1 m^2), ε_c is the emissivity of the condenser (here it is 0.94), σ is Stephan-Boltzmann constant (5.67 × 10^{-8} W m^{-2} K^{-4}), T_c [K] is the temperature of the condenser, and R_{sw} and R_{lw} [W m^{-2}] are the incoming short-wave radiation (i.e., surface solar radiation downwards) and incoming long-wave radiation (i.e., surface thermal radiation downwards)
P_cond	W	Conductive heat exchange between the condenser surface and the ground. For simplicity, we assumed that the condenser is perfectly insulated from the ground; i.e., P_cond = 0
P_conv	W	Convective heat exchange $P_{conv} = S_c\,(T_a - T_c)\,h$ where S_c is the condenser surface area (here it is 1 m^2), T_a [K] is the ambient temperature at 2 m from the ground, T_c [K] is the temperature of the condenser, and h [W m^{-2} K^{-1}] is the heat transfer coefficient that is estimated based on a semi-empirical equation [37] $h = 5.9 + 4.1\ WS\ (511 + 294)/(511 + T_a)$ and here WS [m s^{-1}] is the prevailing horizontal wind speed at 2 m from the ground.
P_lat	W	Latent heat released by the condensation or desublimation of water $P_{lat} = \begin{cases} L_{vw}\frac{dm_w}{dt} T_c > 0°C \\ L_{vi}\frac{dm_i}{dt} T_c < 0°C \end{cases}$ where L_vw [J kg^{-1}] is the specific latent heat of water vaporization and L_{vi} [J kg^{-1}] is specific latent heat of water desublimation. Here, dm_w/dt is the change rate of water whereas dm_i/dt is the change rate of ice

In practice, the wettability of the surface affects vapor pressure P_c directly above it. In other words, P_c is lower over a wet surface; and thus, condensation may take place even if $T_\mathrm{c} > T_\mathrm{d}$ (e.g., [15]). According to the model setup, Equation (A3) assumes irreversible condensation; i.e., there is no evaporation or sublimation during daytime even if $T_\mathrm{c} > T_\mathrm{a}$. Furthermore, the model simulation resets

the cumulative values for water and ice condensation at noon. and takes the preceding maximum value of $m_w + m_i$ as the representative daily yield. This way, the model simulation replicates the daily manual dew water collection of the condensed water around sunrise; i.e., after which T_c is often above the dew point temperature.

Table A2. A list of nomenclature.

Parameter	Unit	Description
α		Albedo of condenser sheet
C_a	J kg^{-1} K^{-1}	Specific heat capacity of air
C_c	J kg^{-1} K^{-1}	Specific heat capacity of the condenser
C_i	J kg^{-1} K^{-1}	Specific heat capacity of ice
C_w	J kg^{-1} K^{-1}	Specific heat capacity of water
DP	K	Dew point temperature
h	W K^{-1} m^{-2}	Heat transfer coefficient
k	Per s^{-1}	Mass transfer coefficient
L_{vi}	J kg^{-1}	Specific latent heat of desublimation for water
L_{vw}	J kg^{-1}	Specific latent heat of vaporization for water
L_{wi}	J kg^{-1}	Latent heat of fusion
m_c	kg	Mass of the condenser
m_i	kg	Mass of ice
m_w	kg	Mass of water
p	Pa	Atmospheric air pressure
p_c	Pa	Vapour pressure over condenser
p_{sat}	Pa	Saturation pressure of water
P_{cond}	W	Conductive heat exchange between the condenser surface and the ground
P_{conv}	W	Convective heat exchange
P_{lat}	W	Latent heat released by the condensation or desublimation of water
P_{rad}	W	Heat exchange due to incoming and outgoing radiation
R_{lw}	W m^2	Surface thermal radiation downwards
R_{sw}	W m^2	Surface solar radiation downwards
S_c	m^2	Surface area of condenser
T_a	K	Ambient temperature at 2 m
T_c	K	Temperature of the condenser
U_{10}	m s^{-1}	Horizontal wind speed component at 10 m
V_{10}	m s^{-1}	Horizontal wind speed component at 10 m
WS	m s^{-1}	Prevailing horizontal wind speed at 2 m
z_0	m	Surface roughness
δ_c	mm	Condenser sheet thickness
ε_c		Emissivity of condenser sheet
γ	Pa K^{-1}	Psychrometric constant
σ	W m^{-2} k^{-4}	Stefan–Boltzmann constant

Appendix A.2. Meteorological Input Data

The meteorological input data-base includes horizontal and vertical wind components (U_{10} and V_{10}) at 2 m, surface roughness (z_0), ambient temperature and dew point (T_a and D_P) at 2 m, and short-wave and long-wave surface solar radiation (R_{sw} and R_{lw}). The input database was downloaded from the European Centre for Medium Range Weather Forecast (ECMWF) Interim Reanalysis (ERA-Interim), which is a global atmospheric reanalysis that is available from 1 January 1979 to 31 August 2019 and it has been superseded by the ERA5 reanalysis. ERA-Interim is a reanalysis of the global atmosphere covering the data-rich period since 1979 and continuing in real-time [61,62], which has a horizontal resolution of 0.75 (approximately 80 km) and 60 vertical levels. The reanalysis combines available data sources (satellite, radiosondes, aircraft, buoy data, stations, etc.) into a coherent and balanced form of the atmospheric dynamic and thermodynamic state [63].

The ECMWF database is differentiated into 3 main categories: reanalysis, instantaneous forecast, and accumulated forecast. In our case, U_{10}, V_{10}, Ta, and D_P were obtained from the reanalysis fields at

00:00, 06:00, 12:00, and 18:00 UTC whereas, at 03:00, 09:00, 15:00, and 21:00 UTC they were instantaneous forecasted fields. Both the forecasted and the reanalysis fields provided 3 hourly time resolution. According to the ECMWF database, the horizontal wind components (U_{10} and V_{10}) are provided at 10 m. Therefore, the wind speed at 2 m was calculated by using a logarithmic wind profile

$$WS = \frac{log\left(\frac{2+z_0}{z_0}\right)}{log\left(\frac{10+z_0}{z_0}\right)} \sqrt{U_{10}^2+V_{10}^2} \quad \text{(A4)}$$

where z_0 is the surface roughness and U_{10} and V_{10} are the horizontal wind speed components at 10 m. It is important to understand that Equation (A4) is a simple equation that is valid during certain conditions. For instance, in stable conditions (such as at night) Equation (A4) overestimates wind speed at 2 m whereas in unstable conditions Equation (A4) underestimates the wind speed at 2 m.

According to the ECMWF database, z_0 was obtained as an instanton forecast parameter whereas R_{sw} and R_{lw} were accumulated forecasted fields. The mean R_{sw} and R_{lw} in a time interval are obtained by taking the difference of the accumulated values between the corresponding time steps divided by the time difference in seconds. The result is a mean value for that time interval 00:00 or 12:00. All input parameters had a horizontal resolution of 0.25 degrees (approximately 30 km).

Appendix A.3. Example of a Detailed Model Simulation Output

To show the model output results in detail, we selected Irbid station from 23–28 September 2008 (Figure A1), which had the maximum dew yield in this period based on the model simulation result. This station is located in the north of Jordan with about 80 km distance from the Mediterranean Sea. Besides the model simulation output, which includes dew yield and temperature of the condenser sheet (T_c). Figure A1 also shows the corresponding model input: long-wave radiation (R_{lw}), short-wave radiation (R_{sw}), wind speed (WS), ambient temperature (T_a), and dew point (D_P).

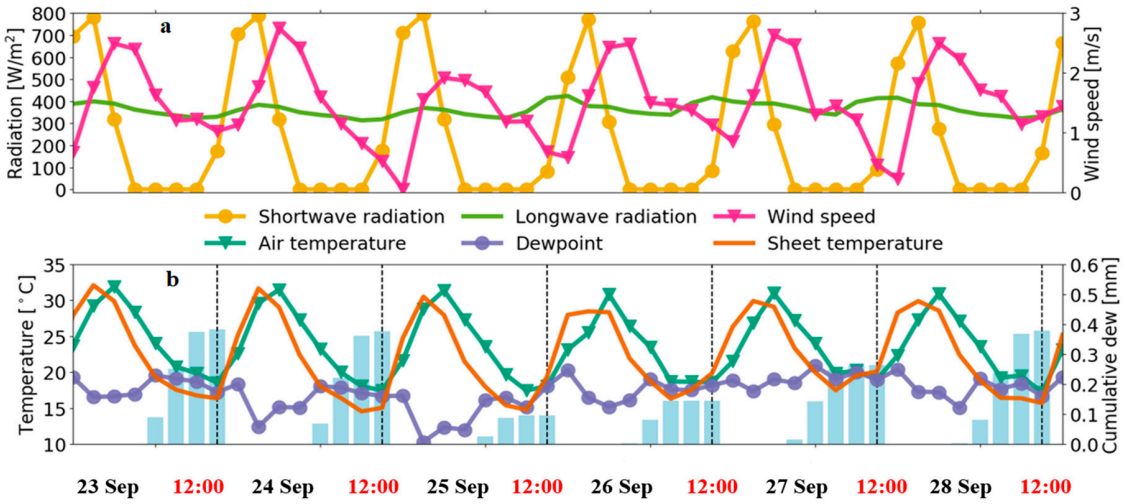

Figure A1. An example model simulation for dew formation from 23–28 September 2001 at Irbid, Jordan. (**a**) the short-wave and long-wave radiation (left y-axis) and wind speed (right y-axis) whereas (**b**) the cumulative dew formation on the condenser (bars linked to the y-axis right axis) and the ambient temperature, dew point, and condenser sheet temperature (left y-axis).

Here it is clearly shown that condensation occurs when $T_c < D_P$ and WS is mostly less than 1 m s^{-1}. In general, at this station, the dew formation is expected to start in the evening (around 18:00) and continues to the next morning (until 06:00). The daily collection of dew occurs at noon. During this period, the total cumulative dew yield is ~2 mm. This dew yield is equivalent to ~2 L collected on a 1 m^2 condenser sheet (i.e., L m^{-2}).

During the daytime, the incoming short-wave radiation from the sun as well as the atmospheric long-wave radiation act to increase the temperature of the condenser sheet. In contrast, during dark periods, the outgoing thermal radiation exceeds the atmospheric long-wave radiation. This one is greatly influenced by cloudiness. For example, the thermal emission by clouds, especially low clouds, increases the incoming thermal radiation at the surface.

References

1. Lindblom, J.; Nordell, B. Water production by underground condensation of humid air. *Desalination* **2006**, *189*, 248–260. [CrossRef]
2. Lekouch, I.; Muselli, M.; Kabbachi, B.; Ouazzani, J.; MelnytchoukMilimouk, I.; Beysens, D. Dew, fog, and rain as supplementary sources of water in southwestern Morocco. *Energy* **2011**, *36*, 2257–2265. [CrossRef]
3. Khalil, B.; Adamowski, J.; Shabbir, A.; Jang, C.; Rojas, M.; Reilly, K.; OzgaZielinski, B. A review: Dew water collection from radiative passive collectors to recent developments of active collectors, Sustain. *Water Resour. Manag.* **2016**, *2*, 71–86. [CrossRef]
4. MaestreValero, J.F.; MartinezAlvarez, V.; Baille, A.; MartínGórriz, B.; GallegoElvira, B. Comparative analysis of two polyethylene foil materials for dew harvesting in a semiarid climate. *J. Hydrol.* **2011**, *410*, 84–91. [CrossRef]
5. Mileta, M.; Beysens, D.; Nikolayev, V.; Milimouk, I.; Clus, O.; Muselli, M. Fog and Dew Collection Projects in Croatia. Available online: https://arxiv.org/ftp/arxiv/papers/0707/0707.2931.pdf (accessed on 22 November 2019).
6. Agam, N.; Berliner, P.R. Dew formation and water vapor adsorption in semiarid environments—A review. *J. Arid Environ.* **2006**, *65*, 572–590. [CrossRef]
7. Kidron, G.J.; Herrnstadt, I.; Barzilay, E. The role of dew as a moisture source for sand microbiotic crusts in the Negev Desert, Israel. *J. Arid Environ.* **2002**, *52*, 517–533. [CrossRef]
8. Nikolayev, V.S.; Beysens, D.; Gioda, A.; Milimouka, I.; Katiushin, E.; Morel, J.P. Water recovery from dew. *J. Hydrol.* **1996**, *182*, 19–35. [CrossRef]
9. Nilsson, T.M.J.; Vargas, W.E.; Niklasson, G.A.; Granqvist, C.G. Condensation of water by radiative cooling. *Ren. Energy* **1994**, *5*, 310–317. [CrossRef]
10. Rajvanshi, A.K. Large scale dew collection as a source of fresh water supply. *Desalination* **1981**, *36*, 299–306. [CrossRef]
11. Jumikis, A.R. Aerial wells: Secondary source of water. *Soil Sci.* **1965**, *100*, 83–95. [CrossRef]
12. Hamed, A.M.; Kabeel, A.E.; Zeidan, E.S.B.; Aly, A.A. A technical review on the extraction of water from atmospheric air in arid zones. *Int. J. Heat Mass Trans.* **2010**, *4*, 213–228.
13. Beysens, D.; Milimouk, I.; Nikolayev, V.; Muselli, M.; Marcillat, J. Using radiative cooling to condense atmospheric vapor: A study to improve water yield. *J. Hydrol.* **2003**, *276*, 111. [CrossRef]
14. Beysens, D.; Muselli, M.; Nikolayev, V.; Narhe, R.; Milimouk, I. Measurement and modelling of dew in island, coastal and alpine areas. *Atmos. Res.* **2005**, *73*, 122. [CrossRef]
15. Beysens, D. The formation of dew. *Atmos. Res.* **1995**, *39*, 215–237. [CrossRef]
16. Muselli, M.; Beysens, D.; Marcillat, J.; Milimouk, I.; Nilsson, T.; Louche, A. Dew water collector for potable water in Ajaccio (Corsica Island, France). *Atmos. Res.* **2002**, *64*, 297–312. [CrossRef]
17. Raman, C.R.V.; Venkatraman, S.; Krishnamurthy, V. Dew ver India and Its Contribution to Winter-Crop Water Balance. *Agric. For. Meteorol.* **1973**, *11*, 17–35. [CrossRef]
18. Beysens, D.; Muselli, M.; Milimouk, I.; Ohayone, C.; Berkowicz, S.M.; Soyeuxg, E.; Mileta, M.; Ortega, P. Application of passive radiative cooling for dew condensation. *Energy* **2006**, *31*, 1967–1979. [CrossRef]
19. Beysens, D. Dew nucleation and growth. *C. R. Phys.* **2006**, *7*, 1082–1100. [CrossRef]
20. Alnaser, W.E.; Barakat, A. Use of condensed water vapour from the atmosphere for irrigation in Bahrain. *Appl. Energy* **2000**, *65*, 318. [CrossRef]
21. Beysens, D.; Ohayon, C.; Muselli, M.; Clus, O. Chemical and biological characteristics of dew and rain water in an urban coastal area (Bordeaux, France). *Atmos. Environ.* **2006**, *40*, 3710–3723. [CrossRef]
22. Beysens, D.; Clus, O.; Mileta, M.; Milimouk, I.; Muselli, M.; Nikolayev, V.S. Collecting dew as a water source on small islands: The dew equipment for water project in (Croatia). *Energy* **2007**, *32*, 1032–1037. [CrossRef]

23. Galek, G.; Sobik, M.; Blas, M.; Polkowska, Z.; Cichala-Kamrowska, K. Dew formation and chemistry near a motorway in Poland. *Pure Appl. Geophys.* **2012**, *169*, 1053–1066. [CrossRef]
24. Gałek, G.; Sobik, M.; Błaś, M.; Polkowska, Ż.; Cichała-Kamrowska, K.; Wałaszek, K. Dew and hoarfrost frequency, formation efficiency and chemistry in Wroclaw, Poland. *Atmos. Res.* **2015**, *151*, 120–129. [CrossRef]
25. Jiries, A. Chemical composition of dew in Amman, Jordan. *Atmos. Res.* **2001**, *57*, 261–268. [CrossRef]
26. Lekouch, I.; Mileta, M.; Muselli, M.; Milimouk-Melnytchouk, I.; Šojat, V.; Kabbachi, B.; Beysens, D. Comparative chemical analysis of dew and rain water. *Atmos. Res.* **2010**, *95*, 224–234. [CrossRef]
27. Muselli, M.; Beysens, D.; Milimouk, I. A comparative study of two large radiative dew water condensers. *J. Arid Environ.* **2006**, *64*, 54–76. [CrossRef]
28. Odeh, I.; Arar, S.; Al-Hunaiti, A.; Sa'aydeh, H.; Hammad, G.; Duplissy, J.; Vuollekoski, H.; Korpela, A.; Petäjä, T.; Kulmala, M.; et al. Chemical investigation and quality of urban dew collection with dust precipitation. *Environ. Sci. Pollut. Res.* **2017**, *24*, 12312–12318. [CrossRef]
29. Okochi, H.; Kataniwa, M.; Sugimoto, D.; Igawa, M. Enhanced dissolution of volatile organic compounds into urban dew water collected in Yokohama, Japan. *Atmos. Environ.* **2005**, *39*, 6027–6036. [CrossRef]
30. Polkowska, Ż.; Błaś, M.; Klimaszewska, K.; Sobik, M.; Małek, S.; Namieśnik, J. Chemical characterization of dew water collected in different geographic regions of Poland. *Sensors* **2008**, *8*, 4006–4032. [CrossRef]
31. Shachak, M.; Leeper, A.; Degen, A.A. Effect of population density on water influx and distribution in the desert snail *Trochoidea seetzenii*. *Ecoscience* **2002**, *9*, 287–292. [CrossRef]
32. Zangvil, A. Six years of dew observations in the Negev Desert, Israel. *J. Arid Environ.* **1996**, *32*, 361–371. [CrossRef]
33. Clus, O.; Ortega, P.; Muselli, M.; Milimouk, I.; Beysens, D. Study of dew water collection in humid tropical islands. *J. Hydrol.* **2008**, *361*, 159–171. [CrossRef]
34. Kidron, G.J. Altitude dependent dew and fog in the Negev Desert, Israel. *Agric. For. Meteorol.* **1999**, *96*, 1–8. [CrossRef]
35. Leopold, L.B. Dew as a source of plant moisture. *Pac. Sci.* **1952**, *6*, 259–261.
36. Muselli, M.; Beysens, D.; Mileta, M.; Milimouk, I. Dew and rain water collection in the Dalmatian Coast, Croatia. *Atmos. Res.* **2009**, *92*, 455–463. [CrossRef]
37. Richards, K. Observation and simulation of dew in rural and urban environments. *Prog. Phys. Geogr.* **2004**, *28*, 76–94. [CrossRef]
38. Sharan, G. Dew Yield from Passive Condensers in a Coastal Arid Area: Kutch. Available online: http://vslir.iima.ac.in:8080/jspui/bitstream/11718/6362/1/2005-01-05gsharan.pdf (accessed on 22 November 2019).
39. Sharan, G.; Shah, R.; Millimouk-Melnythouk, I.; Beysens, D. Roofs as Dew Collectors: Corrugated Galvanized Iron Roofs in Kothara and Suthari (NW India). In Proceedings of the Fourth International Conference on Fog, Fog Collection and Dew, La Serena, Chile, 22–27 July 2007.
40. Ye, Y.; Zhou, K.; Song, L.; Jin, J.; Peng, S. Dew amount and its correlation with meteorological factors in urban landscapes of Guangzhou, China. *Atmos. Res.* **2007**, *86*, 21–29. [CrossRef]
41. Vuollekoski, H.; Vogt, M.; Sinclair, V.A.; Duplissy, J.; Järvinen, H.; Kyrö, E.; Makkonen, R.; Petäjä, T.; Prisle, N.L.; Räisänen, P.; et al. Estimates of global dew collection potential on artificial surfaces. *Hydrol. Earth Syst. Sci.* **2015**, *19*, 601–613. [CrossRef]
42. Tomaszkiewicz, M.; Abou Najm, M.; Beysens, D.; Alameddine, I.; El-Fadel, M. Dew as a sustainable non-conventional water resource: A critical review. *Environ. Rev.* **2015**, *23*, 425–442. [CrossRef]
43. Monteith, J.L. Dew. *Q. J. R. Meteorol. Soc.* **1957**, *83*, 322–341. [CrossRef]
44. Beysens, D. Estimating dew yield worldwide from a few meteo data. *Atmos. Res.* **2016**, *167*, 146–155. [CrossRef]
45. Gandhisan, P.; Abualhamayel, H.I. Modelling and testing of a dew collection system. *Desalination* **2005**, *18*, 47–51. [CrossRef]
46. Pedro, M.J., Jr.; Gillespie, T.J. Estimating dew duration. I. Utilizing micrometeorological data. *Agric. Meteorol.* **1981**, *25*, 283–296. [CrossRef]
47. Nilsson, T. Initial experiments on dew collection in Sweden and Tanzania. *Sol. Energy Mater. Sol. Cells* **1996**, *40*, 23–32. [CrossRef]
48. Tomaszkiewicz, M.; Abou Najm, M.; Beysens, D.; Alameddine, I.; Zeid, E.B.; El-Fadel, M. Projected climate change impacts upon dew yield in the Mediterranean basin. *Sci. Total Environ.* **2016**, *566*, 1339–1348. [CrossRef]

49. Nikolayev, V.S.; Beysens, D.; Muselli, M. A computer model for assessing dew/frost surface deposition. In Proceedings of the Second International Conference on Fog and Fog Collection, St John's, NL, Canada, 15–20 July 2001; pp. 333–336.
50. Jacobs, A.F.G.; Heusinkveld, B.G.; Berkowicz, S.M. Passive dew collection in a grassland area, The Netherlands. *Atmos. Res.* **2008**, *87*, 377–385. [CrossRef]
51. Jorge Ernesto, A.T.; Jose Jasson, F.P. Winter dew harvest in Mexico City. *Atmosphere* **2016**, *7*, 2. [CrossRef]
52. Abdulla, F. 21st Century Climate Change Projections of Precipitation and Temperature in Jordan. 1st International Conference on Optimization-Driven Architectural Design (OPTARCH 2019). *Proced. Manuf.* **2020**, *44*, 197–204. [CrossRef]
53. Freiwan, M.; Kadioglub, M. Climate variability in Jordan. *Int. J. Climatol.* **2008**, *28*, 69–89. [CrossRef]
54. Hamdy, A.; Lacirignola, C. Mediterranean water resources: Major challenges towards the 21st century. In Proceedings of the International Seminar on Mediterranean Water Resources: Major Challenges Towards the 21st Century, Egypt, Cairo, 1–5 March 1999.
55. Hadadin, N. Dams in Jordan current and future perspective. *Can. J. Pure Appl. Sci.* **2015**, *9*, 3279–3290.
56. Notaro, M.; Yu, Y.; Kalashnikova, O.V. Regime shift in Arabian dust activity, triggered by persistent Fertile Crescent drought. *J. Geophys. Res. Atmos.* **2015**, *10*, 229. [CrossRef]
57. Rezazadeh, M.; Irannejad, P.; Shao, Y. Climatology of the Middle East dust events. *Aeol. Res.* **2013**, *10*, 103–109. [CrossRef]
58. Pohlert, T. *Non-Parametric Trend Tests and Change-Point Detection*; Creative Commons—CC BY-ND 4: Mountain View, CA, USA, 2016; pp. 2–17.
59. Satheesh, S.K.; Deepshikha, S.; Srinivasan, J. Impact of dust aerosols on Earth–atmosphere clear-sky albedo and its short wave radiative forcing over African and Arabian regions. *Int. J. Remote Sens.* **2006**, *27*, 1691–1706. [CrossRef]
60. Givati, A.; Rosenfeld, D. Possible impacts of anthropogenic aerosols on water resources of the Jordan River and the Sea of Galilee. *Water Ressour. Res.* **2007**, *43*, W10419. [CrossRef]
61. Berrisford, P.; Dee, D.; Poli, P.; Brugge, R.; Fielding, K.; Fuentes, M.; Kallberg, P.; Kobayashi, S.; Uppala, S.; Simmons, A. ERA report series. In *The ERA-Interim Archive*; ECMWF—European Centre for Medium-Range Weather Forecasts: Shinfield Park, Reading, UK, 2011; Volume 2.
62. Dee, D.P.; Uppala, S.M.; Simmons, A.J.; Berrisford, P.; Poli, P.; Kobayashi, S.; Andrae, U.; Balmaseda, M.A.; Balsamo, G.; Bauer, P.; et al. The ERA-Interim reanalysis: Configuration and performance of the data assimilation system. *Q. J. R. Meteorol. Soc.* **2011**, *137*, 553–597. [CrossRef]
63. Tampkins, A. *A Brief. Introduction1 to Retrieving ERA Interim via the Web and Webapi*; ECMWF—European Centre for Medium-Range Weather Forecasts: Shinfield Park, Reading, UK, 2017.